



HHS Public Access

Author manuscript

IEEE ASME Trans Mechatron. Author manuscript; available in PMC 2018 February 01.

Published in final edited form as:

IEEE ASME Trans Mechatron. 2017 February ; 22(1): 115–126. doi:10.1109/TMECH.2016.2618362.

MR Safe Robot, FDA Clearance, Safety and Feasibility Prostate Biopsy Clinical Trial

Dan Stoianovici¹, Chunwoo Kim¹, Doru Petrisor¹, Changhan Jun¹, Sunghwan Lim¹, Mark W. Ball¹, Ashley Ross¹, Katarzyna J. Macura², and Mohamad Allaf¹

¹Urology Department, Johns Hopkins University Baltimore, MD

²Radiology Department, Johns Hopkins University, Baltimore, MD

Abstract

Compatibility of mechatronic devices with the MR environment has been a very challenging engineering task. After over a decade of developments, we report the successful translation to clinical trials of our MR Safe robot technology.

MrBot is a 6-degree-of-freedom, pneumatically actuated robot for transperineal prostate percutaneous access, built exclusively of electrically nonconductive and nonmagnetic materials. Its extensive pre-clinical tests have been previously reported. Here, we present the latest technology developments, an overview of the regulatory protocols, and technically related results of the clinical trial.

The FDA has approved the MrBot for the biopsy trial, which was successfully performed in 5 patients. With no trajectory corrections, and no unsuccessful attempts to target a site, the robot achieved an MRI based needle targeting accuracy of 2.55 mm.

To the best of our knowledge, this is the first robot approved by the FDA for the MR environment. The results confirm that it is possible to perform safe and accurate robotic manipulation in the MRI scanner, and the development of MR Safe robots is no longer a daunting technical challenge.

Index Terms

Medical robotics; MR Safe; MRI compatible; robot; pneumatic; motor; FDA; prostate biopsy; clinical trial

I. Introduction

Needle biopsy is a regularly performed procedure required to diagnose prostate cancer (PCa). The most common method is transrectal ultrasound (TRUS) guided. Yet, standard

Personal use is permitted, but republication/redistribution requires IEEE permission. See http://www.ieee.org/publications_standards/publications/rights/index.html for more information.

Corresponding author: Dan Stoianovici, phone: 410-550-1980, dss@jhu.edu.

Disclosure

Under a licensing agreement between Samsung and the Johns Hopkins University, Dr. Stoianovici has received income on an invention described in this article. This arrangement has been reviewed and approved by the JHU in accordance with its conflict of interest policies.

gray-scale ultrasound is unreliable in differentiating PCa from normal gland tissues; therefore needle guidance is usually performed without direct visualization of the cancer [1]. The biopsy relies instead on untargeted, uniformly distributed schemata. These often lead to the detection of clinically insignificant tumors (over-diagnosis) and/or miss significant cancers (i.e. >0.5mL) (under-diagnosis) [2, 3].

An emerging potential solution is to use an imaging modality that may depict cancer suspicious regions (CSR) to target the biopsy, such as magnetic resonance imaging (MRI) [4]. Although MRI methods still have shortcomings, they could point to abnormalities that should be biopsied [5].

Guiding the biopsy based on MRI can be accomplished with indirect or direct guidance methods [6], both having potential advantages. With indirect methods, the MRI is acquired prior to biopsy, and the MRI is subsequently registered (fused) to the interventional TRUS imaging to hint the CSR locations to biopsy (MRI-TRUS Fusion [7]). Direct MRI guidance uses the MRI alone to define the CSR and guide the biopsy. This circumvents targeting errors related to the registration and temporal differences. Fusion biopsy, however, is a non-disruptive advance over the standard TRUS technique, is logistically simpler than the direct method, and clinical studies have already shown approx. 30% increase in the detection of high-risk cancers than untargeted methods [8, 9]. However, targeting accuracy relative to MRI is unknown, and it remains questionable if this method is sufficiently accurate.

On the other side, direct methods are potentially more accurate in terms of CSR targeting but only few procedures have been performed in men, because special devices are needed to help the physician perform the biopsy in the MR environment [10, 11].

Devices for the MR have been initially classified as MRI Compatible or Incompatible, as early as 1993 [12]. While the name stuck, there was no formal definition and the classification was insufficiently descriptive [13, 14]. Instead, standards such as the American Society for Testing and Materials (ASTM) classify (ASTM F2503) devices for the MR environment (Table 1), and set a series of tests that these should meet (ASTM F2052, F2213, F2182, F2119). Most importantly, for clinical use in the United States compliance to these standards is mandated by the Food and Drug Administration (FDA).

The standard points out rationally that devices made exclusively of nonconductive, nonmetallic, and nonmagnetic materials pose no known hazards in the MR environment. The standard also sets the regulatory basis for the determination of MRI safety based on this underlying scientific rationale.

Since testing a device in all MR environments is unfeasible, the standard practically excludes devices that use electricity from the MR Safe category. Several research teams have demonstrated that electrical devices (MR Conditional) can be safely used in the MRI [15, 16]. Since one would not have to use a device in all MR environments, proper tests in the MR equipment of choice could make the MR Conditional device a useful clinical instrument for the specific procedure. Nevertheless, devices that meet the MR Safe standard require less testing for a wider application range. Therefore, the preferential choice when developing a

device for the MR is MR Safe, because this facilitates clinical translation under the regulatory protocols and a broader dissemination.

The development of devices that may operate accurately and safely in the MR environment without interfering with the functionality of the imager has been a very challenging engineering task [17]. As such, initial devices developed for direct MRI guided procedures were manually operated [18–20]. These have the merit of bringing the procedure first to clinical trials. Following research pursued the development of remotely controlled and robotic devices to facilitate the procedure. These required additional developments related to sensing and actuation, since most of the components traditionally used in robotics are MR Unsafe (e.g. electromagnetic motors).

Technical developments of over a decade of research in the field have enabled building several MR Conditional [15, 21–26] and MR Safe robots [14, 27–32]. Yet few have reached the clinical trial stage [33].

Perhaps the first robot to guide a needle in a prostate gland under direct MRI guidance has been reported in 2010 by the University of Utrecht, The Netherlands [34]. The robot is a 5-degrees-of-freedom (DoF) needle-guide device actuated pneumatically. The ASTM 2503 classification was not given, but due to the metallic components used is probably MR Conditional. The robot was used in a 1.5T scanner to transperineally implant several golden seeds in one patient and the procedure was successful.

The following year, also in the Netherlands, the Nijmegen Medical Centre reported the first direct MRI guided prostate biopsy [35]. Ten patients underwent transrectal biopsy procedures in a 3.0T scanner. A remote controlled 5-DoF system using pneumatic turbines but reportedly no position encoders were used. The ASTM classification of the device was not given, but the system could have been MR Safe. The procedures were successful and PCa was sampled at biopsy in several patients.

Also reported in 2011 was a series of 20 patients who underwent direct MRI guided prostate biopsy in Frankfurt, Germany [36] with the Innomedic (Herxheim, Germany) robot, company which unfortunately is no longer active. This has been a marvel of German engineering with very ingenious pneumatic actuators, perhaps MR Safe [27]. A limitation of the clinical study was derived from the robot, which could only operate the needle about the Anterior-Posterior direction, so that the biopsy had to be performed on the unusual, deeper, transgluteal path. All cases were safe, and the procedures were successful in accurately sampling the prostate in 19 patients.

Most recently, in 2014 the Harvard Medical School, Boston, MA reported a study on 30 patients with a 2-DoF robotic motorized needle guide template for transperineal prostate biopsy in a 3.0T scanner [37]. The ASTM standard was not used [26], but the robot uses piezoelectric actuation probably classifying as MR Conditional. Procedures were successful, without severe adverse events, and tissue samples from targeted lesions were collected in all cases. Workflow times were well detailed as well as a comparison of the manual and robotic approaches [38].

With respect to the regulatory protocols for clinical trials, all four devices described above have been cleared by the medical research ethics committees of the respective institutions. The Innomedic was commercially available and was marked MR Compatible in the European Community. In all cases, there were no Food and Drug Administration (FDA) or other superseding administration approvals.

Overall, several MR Conditional and MR Safe devices tested pre-clinically have now demonstrated that robotic operation in the MR environment is possible [14, 15, 21–25, 27–32]. Few devices that reached clinical trial stages showed that direct MRI guided procedures are feasible [20, 34, 35, 37], within certain limitations.

In this study we use a robot structure (MrBot [30]) that was developed based on our MR Safe pneumatic step motor (PneuStep) and optical encoding technologies [29], and extensively tested preclinically [31, 32, 39]. The MrBot was initially built for seed brachytherapy, as a showcase of technology that can operate fully automatically with no human intervention in the MRI scanner. Preclinically this was very successful, but brachytherapy and full robotic operation were not enablers for immediate clinical translation. Therefore, we opted for a biopsy procedure and scaled down the system to manual needle insertion.

Here, we present how the MrBot was adapted for biopsy, a novel way of setting the depth of needle insertion, image-to-robot registration, an overview of the regulatory protocols, and a summary of the safety and feasibility clinical trial.

Relative to previous robotics research for the MR environment this report presents additional technology and control safety features, ASTM 2503 device classifications, and communicates our experience with the clinical translation.

II. Materials And Methods

A. The System

The biopsy device is a 5-DoF robotically driven needle-guide and a 1-DoF depth of needle insertion limiter. The system consists of the robot, its controller, and a laptop for image registration and navigation, as shown in Figure 1. The robot goes in the MR scanner room (ACR Zone IV, [41, 42]) and mounts on the MRI table.

A bundle of hoses including pneumatic circuits and optic fibers connect the robot to its controller located outside the MRI room (ACR Zone III). The hoses are passed through a standard access waveguide and attach to the robot with a custom-built optic and pneumatic connector. A registration marker is built within the base of the needle-guide. MRI images are acquired and passed in DICOM (Digital Imaging and Communications in Medicine) format to the laptop over the network.

Images showing the registration marker are used for robot-to-image registration. Target biopsy locations are selected in the MRI, and the points are mapped to robot-space coordinates based on the registration. The robot controller further maps the robot-space to joint-space coordinates using the inverse kinematics of the robot, and controls the actuators

in closed-loop position feedback. This aligns the needle-guide on target for biopsy, locks the location of the needle-guide (non-back-drivable actuators), and sets the position of the depth limiter. The needle is then inserted manually through the guide, up to the limiter. The biopsy is sampled manually, as usual.

B. The Robot

The robot presents the 5-DoF parallel link structure of the original MrBot robot [30] in which the brachytherapy needle-driver [39] was replaced with a newly developed 1-DoF needle-driver for biopsy reported herein. The biopsy needle-driver is an assembly comprising the needle-guide and the depth limiter. The robot and the new needle-driver are presented in Figure 2.

The robot was designed, analyzed, and manufactured with the Creo (PTC, Inc., Needham, MA) software. The 5-DoF structure positions (3-DoF: X, Y, Z axes) and orients (2-DoF: about X, Y axes) the needle-driver assembly with 5 linear actuators, implemented with screw drivers from rotary PneuStep [29] motors (rotary nut, sliding screw). The structure attaches with suction cups to an adapter plate mounted on the MRI table. The height of the robot over the table can be adjusted by the length of the suction cup mounts.

The needle-driver and its schematic are presented in Figure 2b, c. The needle-guide is attached to the base of the driver (the platform driven by the 5-DoF parallel link). A slider block with a stopper/limiter surface is positioned by a 6th PneuStep motor through a screw driver (rotary screw, sliding nut). The needle is passed through the needle-guide until the needle handle touches the stopper, thus limiting the depth of insertion as needed to reach the target, based on the images.

The entire robot is covered with a sterile bag (Universal Medical EZ-3030) so that the only component that has to be sterilized is the needle-guide (guide and its 2 screws). The placement of the bag over the driver is illustrated in Figure 2c, which shows how the components were designed so that the needle-guide attaches over the bag with the 2 screws and the needle handle touches the limiter through the bag.

The robot is electricity-free, uses air pressure for actuation, light for the position sensors, and is entirely made of nonconductive, nonmetallic, and nonmagnetic materials. These are: ABS/PVC Vinyl, Acetal Copolymer, Delrin Acrylic, Epoxy S5H13, Garolite (G-11, LE), Glass, High-Alumina Ceramic, Nylon (6, fabric), Peek 1000, Polycarbonate, Polyetherimide (Ultem 1000), Polyimide, Polysulfone, Polyethersulfone (Radel), Polyurethane, PTFE (Teflon), Sapphire, Silicone Rubber (Vulcanized, RTV), and Torlon Polyamide-imide Thermoplastic. Their electrical resistivity ranges between $2.0 \cdot 10^5$ and 10^{17} [$\Omega \cdot m$] and dielectric strength between 3–40 [kV/mm].

Moreover, at the request of the FDA, the needle-guide which comes in direct contact with the patient and its 2 screws were built of certified biocompatible material (ISO-10993), Radel BL033 and Radel GN086 (GN4-232-1) rods.

Two types of needles were used in the study, both manufactured by Invivo, Pewaukee, WI: 9896-032-02861 (11528), 18Gax150mm Semi-Automatic Biopsy Gun and 9896-032-05281,

18Gax175mm Fully-Automatic Biopsy Gun (shown in Figure 2b). Accordingly, different limiters for the needle-driver were used to accommodate their different handles.

C. Robot Controller

The controller includes a PC running Microsoft Windows 7, a motion control card, electro-pneumatic and electro-optical interfaces, and several safety components (Figure 3). The motion control card (MCC, MC-8000, PMDI, BC, Canada) presents a digital signal processor (DSP) that is responsible for axis-level coordinated motion control in real-time.

The electro-optical interface converts optical quadrature encoded signals from the PneuStep motors to typical electric signals for the MCC [29]. These are implemented with D10 Expert fiber optic sensors (Banner Engineering Corp., Minneapolis, MN, USA). Position feedback signals are used for closed-loop stepper control of each PneuStep axis. Each linear actuator axis is also equipped with a limit switch, also implemented with fiber optic sensors. These are used to home the incremental encoders of the motors. In Figure 2a the robot is shown at its home position, chosen at a central (square) position of the parallel links.

The electro-pneumatic interface includes a driver for the PneuStep motor [29] and pneumatic valves. The driver converts standard step and direction electric signals of the MCC to three electric signals that sequentially actuate three pneumatic direct acting solenoid valves (NVKF334V-5D by SMC Corp., Indianapolis, IN, USA). In turn, these generate pneumatic commutation waves that power the PneuStep motor.

Safety components include a watchdog, emergency stop buttons, and visual alerts, as shown in the block diagram of the robot controller (Figure 3). This system design has been developed according to a Risk Hazard Analysis discussed later in this article. The watchdog includes software and hardware components. The hardware component is used to mitigate software errors that are possibly indeterministic. The software watchdog checks the state of several components of the system, disabling power to the pneumatic valves, should a faulty condition occur. It runs on a separate (time critical) thread and signals its continuous operation to the hardware watchdog, which suspends power after 0.1s of software watchdog inactivity.

Visual signs are used to signal the operation state of the robot. Two Emergency Stop buttons disable the system and suspend the pneumatic pressure through a circuit that is separate from the watchdog. One is located in the MRI control room and the other on the MRI table next to the patient, so that one is always in close reach should an emergency situation occur.

The motion control software includes axis-level motion control and robot kinematics software built in Visual C++ (Microsoft Corp, Redmond, WA). Axis-level control is implemented on the MCC is developed based on libraries of the MCC (MCI-SoftLib, PMDI). Robot kinematics has been derived based on link parameters resulting from the Computer Aided Design (CAD) of the robot.

A. Image Registration and Navigation

A high contrast MRI marker system for registration (tubes filled with Radiance[®] MRI Imaging Liquid, Beekley, Bristol, CT) and an MRI coil (using MEDRAD BPX-30, Warrendale, PA) are attached to the needle-driver base. MRI of the marker was obtained with a 3 dimensional (3D) gradient recalled echo (GRE) T1-weighted sequence (Marker Scan) with the following parameters: TR/TE = 8.85/1.86 msec, flip angle 14.8, slice thickness 1.2 mm, interslice gap 0, matrix 320×320 , FOV 38×38 cm; No. of averages: 1.

The imaging software was implemented on the laptop based on the Amira Visualization application (Visage Imaging, Inc., San Diego, CA) with custom C++ modules. DICOM images were acquired over the network.

Image-to-robot registration was performed based on the image-to-model registration method. For this, the marker model is aligned with its corresponding marker-image so that the two are superimposed, as shown in Figure 4. By superimposing the two markers their spaces are registered one to another. As such, points selected in the MRI may be mapped to the robot coordinate system (CSys).

The registration marker consists of five geometric features (Figure 4): three line markers (M_1 , M_2 , M_3), an ellipse (E), and a small arc (not shown, next to the needle-guide). Explicitly, the image-to-model registration is performed using a custom method that performs the alignment preferentially along principal directions of the marker system, as follows:

- a. Segment the images of line markers M_1 , M_2 , and the ellipse (E) by selecting a point on the MRI that belongs to each marker, and use a region growing algorithm (with properly selected threshold level) to determine all voxels that belong to each marker.
- b. Fit the voxels of M_1 , M_2 to a plane P_{YZ} by principal component analysis (PCA). The X axis of the robot CSys (see also Figure 2b) is aligned to the normal of this plane, by design. The positive direction is on the side of the ellipse marker E.
- c. Use PCA to find the principal direction of the voxels in M_1 and M_2 . This gives the direction of the robot CSys Z axis, by design. The direction is chosen so that the Z axis points away from the needle-guide, visually shown by the 5th marker.
- d. Project the voxels belonging to the ellipse marker E to plane P_{YZ} and fit them to a line L_E . Likewise, fit the voxels of M_1 , M_2 to lines L_1 respectively L_2 .
- e. Intersect L_E with L_1 and L_2 to determine points P_1 , P_2 , and then point P at their middle.
- f. The center O of the robot CSys is then located at a constant distance from P along the Z axis, by design. With the directions from steps b and c above, this fully defines the location and orientation of the robot CSys relative to the image, therefore the homogeneous registration ${}^R_I T$.

The third line marker is used to verify the registration, as follows:

- a. Segment the image of line marker M_3 and find L_{3I} in image CSys by PCA, as before.
- b. Transform line L_{3I} to the robot from the image ${}^I L_{3I}$ to the robot ${}^R L_{3I}$ CSys (based on ${}^R T_I$)
- c. The equation of the model line L_3 in robot CSys ${}^R L_{3M}$ is known by design.
- d. Find its intersection of ${}^R L_{3I}$ and ${}^R L_{3M}$ with the XY plane as points Q_I respectively Q_M .
- e. Measure the:
 - Angular registration error as the angle between ${}^R L_{3I}$ and ${}^R L_{3M}$.
 - Offset registration error as the distance between points Q_I and Q_M .

Calculated once at the beginning of the case, the registration remains valid as long as the robot is not disconnected from the MRI table. Based on the registration mapping (${}^R T_I$), a biopsy point that is selected in the MRI (${}^I P$) is converted to a target point in robot coordinates (${}^R P = {}^R T_I {}^I P$). The direction of the needle is defined by the location of the skin entry point (on the needle-guide) and the selected target point.

The depth of needle insertion is also calculated based on the images and referenced in the robot CSys. The desired depth of needle insertion is calculated by referencing the depth of the needle to the center of the biopsy core slot. The depth is also offset with the forward-fire distance of the needle. With these, the target biopsy point selected in MRI corresponds to the center of the biopsy sample. As such, the limiter sets the depth of insertion short of the target, and the target is reached only after firing the needle, as usual.

As often is the case with parallel link robots, the inverse kinematics is trivial and has an analytic form; the direct kinematics is numerically evaluated. Robot space coordinates are passed to the robot controller, which calculates all 6 joint coordinates based on the inverse kinematics. It then orients the trajectory on target and presets the location of the needle depth limiter.

B. Clinical Protocol Summary

A pilot study of five men with elevated prostate specific antigen, prior negative prostate biopsy, and CSR on MRI was conducted to assess the safety and feasibility of direct MRI guided prostate biopsy with the MrBot robot. The robot and the image-guidance software should be portable between MRI scanner models, even though the best sequences to image the registration markers may have to be tested and custom table adapters may be required. A Siemens TRIO 3T (Tesla) scanner was used with the Siemens TIM body matrix coil, spinal coil and an optional eCoil™ (Medrad, Warrendale, PA).

The robot was placed in the MRI room, connected to the controller, initialized, homed, covered with the sterile bag, and a sterilized needle-guide was mounted. The biopsy needle, a spare, and all other biopsy supplies were prepared.

The patient was placed under general anesthesia, prepared, draped, and a small perineal incision (~1cm) was made to facilitate the insertion of the needle and reduce needle and soft tissue deflections. The robot was placed on the MRI table beside the patient positioned in left lateral decubitus position. The height of the robot over the table was adjusted so that the needle-guide nozzle matched the height of the incision. The robot was manually positioned on the table so that the needle-guide was placed at the skin incision and intuitively oriented to point towards the prostate (with robot at home). The suction cups were engaged to lock the robot in place. The patient was further padded and secured, and clearance within the bore was tested.

The image-to-robot registration was processed, as described above, based on the 3D T1 GRE sequence (Marker Scan). MRI of the pelvis, perineal structures and the robot at a large field of view was performed in a sagittal plane with T2-weighted fast spin-echo images: TR/TE = 3170/80 msec, slice thickness 4 mm, interslice gap 0–1 mm, matrix 384×288 , FOV 40×40 cm, frequency direction anteroposterior, number of excitations = 2, and “distortion correction” parameter ON. The purpose of this scan was to assure adequate alignment of the robot in reference to the prostate. Subsequently, a smaller field of view axial pelvic MRI with T2-weighted fast spin-echo technique was acquired: TR/TE = 5850/95 msec, slice thickness 4 mm, interslice gap 0–1 mm, matrix 320×320 , FOV 32×32 cm, frequency direction anteroposterior, number of excitations = 2, and “distortion correction” parameter ON. This sequence was used to identify CSRs in the prostate. If visible, CSRs were selected in MRI in addition to other sextant locations for targeting during the biopsy procedure. No multi-parametric MRI or other PCa imaging methods were used at the time of biopsy due to the study’s safety and feasibility nature (a study limitation).

To measure the actual targeting errors, needle localization within the gland after firing the biopsy was acquired with a 2D GRE True-FISP sequence, TR/TE 4.66/2.33, flip angle 49, slice thickness 4 mm, number of excitations = 1–2, matrix 320×320 , FOV 30×30 cm.

The skin entry point was slightly shifted laterally to the right or the left side (approx. ± 1 cm, up or down relative to the table) corresponding to the side of the prostate being targeted. This was possible through the same small skin incision (~1cm) given the flexibility of the perineal skin. During the small size clinical trial, we found no limitation in this regard or the prostate size.

For each target, the robot automatically oriented the needle-guide and preset the depth of insertion. Transperineal biopsies were performed by manually inserting the needle through the guide up to the depth of the limiter. Two samples were taken, and after the second the needle was left in place to acquire MRI for location confirmation. The needle was removed before moving to the next biopsy location.

Anonymized images were acquired for the study, and several Case Report Forms were filed before (patient screening, inclusion/exclusion criteria forms), during (procedure parameters form), and after (urologist, radiologist, and pathology report forms) the procedure, at the request of the FDA. The outcome variables of the study include assessment measures of the robotic device, such as the number of unsuccessful attempts to target a site, the time for

device setup on the MRI table, for image registration, to define biopsy locations, to align the needle guide on target, the total time to biopsy one site (including target verification imaging, excluding initial imaging), grades for the operation of the device [1–5, 1 excellent], for image deterioration [1–5, 1 unperceivable], number of trajectory corrections required to target a site, and targeting error measurements.

The needle direction was set to point directly to the target selected in the image, considering that the trajectory of needle insertion will be a straight line. After insertion and firing the biopsy needle, images were acquired with the True-FISP sequence described above. Targeting errors were measured offline in the MRI as a vector distance between the actual imaged location of the fired needle (at the center of the biopsy slot) and the desired target point. Precision and accuracy results were calculated as usual, based on the standard deviation respectively the mean of the respective errors.

C. Overview of the Regulatory Process

An investigational device is a medical device which is the subject of a clinical study designed to evaluate the effectiveness and/or safety of the device. In the United States (US), medical research ethics committees, commonly termed Institutional Review Boards (IRB), have the discretion of approving investigational device studies that they deem to be Non-Significant Risk (NSR) (21 CFR 812 [43]). In this case, there is no requirement to report to the FDA. This is perhaps the mechanism that allowed other devices to be clinically studied in the US based on IRB approvals alone. However, proceeding with an NSR study is at risk, because the FDA can later disagree on the NSR determination. For this, some institutions (including ours) seek the advice of the FDA voluntarily regarding NSR determinations.

An Investigational Device Exemption (IDE) is an FDA approval that allows to undertake clinical investigations of a medical device in order to collect safety and effectiveness data. While NSR studies may proceed without FDA approval, significant risk (SR) studies are required to submit an IDE application and receive approval prior to commencing the clinical study. In industry, the IDE is typically used to support a premarket approval (PMA) application or a premarket notification (510(k)) submission to the FDA. In academic research, the IDE is required under the law to conduct the SR clinical study and in turn by the IRB.

The determination of the NSR vs. SR status is therefore critical and bifurcates the regulatory protocols to follow. The determination is regulated by 21 CFR 812.3m [43]. To determine if a device is SR, the law sets four tests of which three are logically null, so the definition is logically equivalent to: “Significant risk device means an investigational device that presents a potential for serious risk (sR) to the health, safety, or welfare of a subject”. The other parts of the definition (implants, life supporting/sustaining devices, or of substantial importance in diagnosing, curing, mitigating, or treating disease) are probably showing what the framers of this regulation thought were likely to be regarded as SR devices. Determining the potential for serious risk (sR) is done through a Risk Hazard Analysis (RHA), described below.

The first development in the regulatory process is the clinical protocol, because this plays a role in several other components. This is mainly the job of the clinical part of the team with

help from the engineers related to the investigational device. A pivotal component, and second development step is the RHA. This is conducted for the investigational device to use in the specific clinical procedure as described in the clinical protocol. The development of the RHA is mainly the responsibility of the engineering part of the team with help from the clinicians, related to injuries and severities associated with possible hazards.

The FDA has no formal requirements on the RHA. We used the Failure Mode, Effects and Criticality Analysis (FMECA). The likelihood of the hazard occurring was scored against the severity of the hazard to indicate the risk of the occurring hazard according to ISO 14971 and the Association for the Advancement of Medical Instrumentation (AAMI). These were derived based on the formal definition of injury (21 CFR 803.3), on point scales to quantify the severity and likelihood of a hazard, hazard observability, device performance, methods of control, and hazard mitigation. When applied to a hazard event, the method classifies it according to 21 CFR 812.3(m) as impacting/not impacting a serious risk to the health, safety, or welfare of the subject (sR).

The FMECA was applied in Top-Down as well as Bottom-Up analyses. The Top-Down analysis defines all functions of the device, for each identifies all potential failure modes, and for each runs the sR determination described above. The Bottom-Up analysis list all foreseeable causes and combinations of hazard causes, for each determines all foreseeable failure modes, and for each determines the corresponding effects/hazards and runs the sR determination. The collection of the sR results of all hazard events determines the overall SR status of the investigational device. If at least one result is sR, the device is SR.

Besides its decisive role in the regulatory process, we found the RHA to be a valuable development tool, because it pinpoints safety problems, links device failures to risks, and provides a mechanism to mitigate the risks by hardware and software design, alarms, user training, and even patient inclusion-exclusion criteria.

The IDE application was developed and formatted according to 21CFR812.20-38 regulations and FDA recommendations [44]. The report of previous investigations was based on our massive preclinical data with the MrBot [17, 29–32, 39]. Additional data detailed the changes made for the biopsy application, MR Safe tests and classification according to ASTM F2503-13, needle-guide sterilization parameters and ISO-10993 material certifications, and software documentation.

The software documentation followed the Guidance for the Content of Premarket Submissions for Software Contained in Medical Devices [45] and the Off-The-Shelf Software Use in Medical Devices [46]. The software documentation of the IDE application depends on the device's Level of Concern, being major, moderate, or minor. The instructions provide a clear methodology to estimate the severity of injury that the device could inflict on a patient or operator as a result of device failures. The RHA is a component of this determination as well. The analysis for the MrBot in the direct MRI-guided biopsy procedure the Level of Concern was determined to be Moderate and software documentation was filled accordingly.

III. Results

A. Image-to-Robot Registration

Seven registration experiments were conducted to measure the angular and offset registration errors. Precision and accuracy results were calculated as usual, based on the standard deviation respectively the mean of the errors. The results are presented in Table 2.

The knowhow derived in the experiments are:

1. Long registration markers (> approx. 5cm) of tubular cross section (approx. 4mm inner diameter), filled with Beekley MRI contrast, and oriented quasi-normal to the image slices make good registration markers.
2. Using a T2-weighted sequence to image the registration marker may cause registration errors, being susceptible to image shift geometric artifacts related to the MR frequency encoding direction;
3. Registering on the 3D T1-weighted images of the marker and targeting on T2-weighted images of the tissues are appropriate; in addition to other parameters, we found out that the frequency-encoding direction should be the same on both sequences (anteroposterior in our case).
4. When using T2-weighted images, enabling the “distortion correction” parameter helps correcting geometric shift.

B. FDA Approval

The device development and clinical study were performed entirely at our academic institution, with no industry involvement. As such, we exercised the roles of sponsor (typically the manufacturer of the device) and investigators (typically physicians at a hospital).

A Pre-IDE application was first filed to seek the advice of the FDA regarding the SR determination. The FDA has determined that our proposed clinical investigation presents a SR, in accordance with the definition for a SR device in 21 CFR 812.3(m) of the IDE regulation. Therefore, we have been required to submit an IDE application, and receive both FDA and IRB approval before initiating the study.

The IDE application G120104 was filed on April 20, 2012. This was followed by additional questions from the FDA and a notice of disapproval detailing a list of deficiencies. An amended application was filed with the revisions and additional data requested. This has been subsequently approved on August 9, 2012. The robot device was labeled MR Safe according to ASTM F2503. The Johns Hopkins Hospital IRB approved the clinical protocol subsequently.

C. Safety and Feasibility Clinical Trial

Five men underwent direct MRI guided transperineal prostate biopsy assisted by the MrBot device. A photograph of the robot next to the patient in the left lateral decubitus position in the MRI scanner is presented in Figure 5.

The optional eCoil™ was used on the first patient only. The first case was performed with the semi-automatic biopsy needle. Six biopsy sites were targeted and 3 trajectory corrections were necessary. The accuracy and precision were 14.78 mm respectively 3.82 mm. Needle deflection from a straight path was pronounced. The urologists observed that this needle may not have been as sharp as usual.

For the following cases the needle was changed to the fully-automatic type. Moreover, near the midpoint of the insertion stroke, the needle was rotated 180° about its axis to compensate for lateral deflections due to the beveled point [47].

A table mount adapter with a flat top surface was also made to facilitate the positioning of the robot on the table, and an additional structural support bar was placed on the needle-driver (with FDA 5-day notice approval). In these 4 cases, the accuracy and precision of targeting over 30 biopsy sites is presented in Table 3, in 3D as well as in the plane normal to the needle (XY Plane in Figure 4).

The outcomes related to the functionality of the device are listed in Table 4. In case 3, the MRI scanner shut down at the beginning of the procedure. The cause is unknown, but it is possible to be related to a vacuum pump located in the MRI equipment room that operated the mounting suction cups of the robot. To eliminate this possibility, the hospital vacuum system was used instead thereafter. The scanner also lost images from the study in a case, for an unknown cause. Since this was at the end of the case, only the last 3 verification images were lost/unreliable.

No adverse events were noted and all patients tolerated the procedure well. The total time of the procedure, including patient preparation, anesthesia, MRI imaging, and patient wake-up averaged 208 min with a decreasing trend. Even though this was not a study designed to detect PCa, and no special PCa imaging were used interventionally, biopsies confirmed the presence of clinically significant cancer in 2 of the 5 patients.

IV. Discussion and Conclusion

This article reports the successful translation to clinical trials of an MR Safe robot technology that was in the works for over a decade. This was long delayed by the rigorous regulatory protocols that our institution imposes, but overall we believe that the time and efforts were well invested. To the best of our knowledge this is the first robot approved by the FDA for the MR environment. Following all rigors of the process provides proper technology support documentation for applications to follow. The IDE has also been a very instructive experience for our academic research group. We also believe that parts of the regulatory process are essential design tools for medical devices.

An important feature of our device is that it is MR Safe based on a scientifically based rationale of having an electrically nonconductive, nonmetallic, and nonmagnetic composition. Few such robots were built [27, 28], while most of the other use piezoelectric actuation (include electrically conductive, metallic components). Several other researchers have implemented pneumatic actuation, but fell slightly short of the MR Safe classification by using few metallic components [48, 49].

We would like to underscore that excluding conductive components from MRI devices is essential for the clinical translation, at least in the United States. The FDA requires the ASTM F2503 testing, and this uses practically exclusively the scientifically based rationale. The path to clinical translation is therefore easier with an MR Safe robot. Coping with technical challenges related to MRI distortion that electrical actuation entails, and in addition being in a more restrictive class of testing because of the MR Conditional classification is unhelpful.

This report demonstrates that accurate direct MRI guided needle targeting is possible. In this human trial, the robot was capable of 2.97 mm 3D accuracy and 2.55 mm in the plane normal to the needle. For PCa the required accuracy is probably < 5mm, since a clinical significant tumor (0.5 cm^3) has a 5mm radius if spherical. *But staying within the 5mm radius is difficult.* Targeting errors include numerous components which are often cumulative: image geometry errors, registration errors, robot position errors, robot structural deformations under load, and never the less needle deflections. An error component analysis and trying to minimize/mitigate each of the individual components is helpful.

In our case, the preliminary and current results that enabled the needle to reach the target within 5mm are: PneuStep motor (up to 37W) linear step 0.055 mm [29], a stiff parallel-link structure, bench tests of motion 0.076 ± 0.035 mm [31], linear motion in a 7T MRI scanner 0.047 ± 0.053 mm [31], motion repeatability 0.060 mm [30], placing seeds in agar models 0.72 ± 0.36 mm [31] and under 3T MRI guidance 1.2 mm (SD 0.4 mm) [39], targeting under 3T MRI in an animal model with needle accuracy of 2.02 mm (range 0.86–3.18 mm) and seed placement accuracy of 2.50 mm (range 1.45–10.54 mm) [32], and registration errors of 0.25 mm (SD 0.31 mm) reported herein. The image-to-robot registration markers and the method used are presented in details together with our know-how derived experimentally. Even though the method is based on the classic image-to-model registration, our implementation is original, simple, and validated.

But even so, in case one the errors were on the order of 15 mm. A problem that many others also confronted [20, 47, 50, 51] is that needle deflection errors can be sizeable. In our preclinical experiments where accuracy was good, we used symmetric point (diamond) needles. But for the biopsy trial, most biopsy needles (perhaps all MR types) have asymmetric point (beveled). The beveled surface at the needle point acts like a rudder deflecting the needle laterally during insertion [52]. Depending on numerous factors including the depth of needle insertion, needle gauge, model, and type of tissues, deflections can be significant, for example 10% of the insertion depth [47, 52]. This component alone may be sufficiently large to defeat the purpose of the image-guidance itself. New needles or steering methods are therefore in high demand.

The two needles used were from the same company, one semi- and the other fully-automated type. With a semi-automated type, the forward motion of the stylet is manual, while with the fully-automated type both the stylet and subsequent barrel motion are spring loaded. In our case the automated model performed better, but we have no evidence that this was related to the dissimilar automation.

So, we have been able to cope with the needle problem by using a different needle model (still beveled) and reducing the effect of needle deflection by rotating [47, 53] the needle 180° about its axis near the middle of the insertion stroke. Alternatively, one could possibly account for needle deflections in the guidance software [20] (even though this depends on the types of tissues) and/or interactively adjust the trajectory [37]. We could have done so, but here we aimed to perform a controlled study on the robot accuracy (straight on target, no variability).

Our robot presents a 5-DoF parallel link structure to position and orient a needle-guide and a 1-DoF stopper to limit the depth of manual needle insertion. The limiter feature and its arrangement under the sterile bag is novel and reduces the number of sterile components to the needle-guide alone. In most image-guided robots and all 4 that were used clinically [34–37] the depth was decided by the operator, who typically looked up the marks on the needle. This is adequate since accurate control of the needle depth for biopsy is not critical. The length of the biopsy slot (typically 17 mm) is forgiving for errors in depth (perhaps within $(17-10)/2 = \pm 3.5$ mm). For this most needle targeting studies report the normal plane values alone [36, 51]. With our actuated limiter, the depth is also very accurately controlled, as shown by the small difference between the accuracies in 3D (2.97 mm) and normal plane (2.55 mm). The difference is most likely due to needle localization errors caused by the distance between the image slices. The depth automation reduces the workload of the physician and the possibility of errors. Also, the improved depth accuracy could be helpful for other procedures such as ablations where depth may be critical. Overall, we believe that scaling down from the robotic (of the original MrBot [39]) to the manual needle insertion, and having the depth of needle insertion limited robotically, have enabled the regulatory approval of the device based on the RHA.

We believe that the achieved MRI based targeting accuracy of 2.55 mm is outstanding. The only one of the previous four clinical studies that reported targeting errors was with the Innomedic robot [34]. Their median deviation from the needle point to the planned access was 0.9 mm (range, 0.3–1.6 mm). Because this was done with a thicker 15Ga needle with symmetric point, component errors related to the needle were likely smaller, but nevertheless, robotic accuracy was outstanding.

Unlike MRI-TRUS Fusion methods, the accuracy of direct MRI guided biopsy can be quantified, as we report. Fusion methods suffer from the intrinsic inability to verify targeting back in the MRI, since the intervention is not done at the MR scanner. Ideally, with the target being defined in the MRI, targeting verification should be in MRI. Clinical studies to objectively quantify targeting accuracy with fusion methods would be very difficult, and no reports exist to date. In-vitro studies reported that fusion may target clinically significant sized PCa lesions 89% of the time, but > 5mm errors otherwise [51]. Still, numerous clinical trials with the Fusion [7–9] have shown improved cancer detection relative to the TRUS-alone biopsy, and the fusion is clearly more accurate than untargeted methods.

The most recent similar direct MRI guided clinical trial [37, 38] was performed on a larger population. In this, the clinician often made multiple targeting adjustments before taking a

sample. Insertion attempts averaged 1.9 ± 0.7 per biopsy and the accuracy from the best attempt was 2.39 mm. In our case no trajectory corrections were made.

The workspace of the robot was sufficient to cover the prostate in all cases. However, to do so, the robot was initially oriented towards the center of the prostate. A larger angular workspace could make the initial positioning of the robot faster (current setup time 8.4 (SD 3.4) min).

Clinically, the main critique of direct MRI-guided methods, at least at this stage of development, is the lengthy procedure time [37]. This is because it collates several procedures that are normally done independently, including the anesthesia and the MRI which is inherently slow. By itself, the biopsy procedure time/site is on the order of 10 min. Moreover, robotic assistance reduces time compared to the manual Direct MRI guided approach [38].

In trial [37] the needle-guide was manipulated with 2-DoF of translation and the needle pierced the skin at every biopsy location. Instead the MrBot operated the needle through one small (1 cm) perineal skin incision. With 5-DoF, the needle-guide could be translated in all 3 directions and angulated. We found these enabling to target all regions of the prostate and avoiding interference with the pubic arch (zero unsuccessful attempts to target a site). The nozzle of the needle-guide was placed superficially through the incision. We found that the single central incision was sufficient to slightly shift the needle-guide left-and-right (~15mm) based on the elasticity of the skin. We believe that the incision helped to reduce needle based targeting errors by avoiding to pierce the skin.

In conclusion, we have finally been able to take our MR Safe robotic technology to a pilot clinical trial while adhering to all rigors of the regulatory process in the United States. A summary of our experience is included herein, hoping that it will help others navigate the regulatory paths. The study demonstrates that accurate MRI based targeting in the MRI scanner is possible. It also demonstrates that the development of MR Safe robots is no longer a technical challenge. Due to regulatory restrictions, the study was limited to safety and feasibility measures. A new study is needed to assess the clinical significance of accurate targeting.

Acknowledgments

The authors would like to thank Biomedical Engineer John Baxley of the FDA Office of Device Evaluation and his team for their knowledgeable guidance that enabled our small academic research laboratory to successfully sponsor the IDE of the MrBot investigational device. This does not attribute FDA's agreement on the contents of the article or related regulatory policy.

The project described was supported by Award Number RC1EB010936 from the National Institute of Biomedical Imaging and Bioengineering. The content is solely the responsibility of the authors and does not necessarily represent the official views of the NIBIB or the National Institutes of Health.

Biographies

Dan Stoianovici (ASME M' 1994) received the Ph.D. degree from Southern Methodist University, Dallas, TX, in 1996. He is Professor of Urology, Mechanical Engineering,

Neurosurgery, and Oncology at the Johns Hopkins University. He is also the Director of the Urology Robotics Program. His specialty is medical robotics in particular robotic hardware and image-guided robots. His bibliography includes numerous publications and 20 patents of invention. He serves on the editorial boards of the IEEE/ASME TRANSACTIONS on Mechatronics, Journal of Endourology, International Journal of Medical Robotics and Computer Aided Surgery and other cross disciplinary medical-engineering journals.



Chunwoo Kim (S' 2010) received a B.S. degree from Department of Mechanical Aerospace Engineering at Seoul National University in 2008. He received a Ph.D. degree in Mechanical Engineering at Johns Hopkins University in 2014. He is currently with the Healthcare Robot Group, Korea Institute of Science and Technology, Seoul, South Korea. He is a recipient of the Fulbright scholarship and the Prostate Cancer Research Training Award of the United States Department of Defense. His research interests include image-guided robots and medical imaging.



Doru Petrisor (ASME M'2003) received a MS degree in Mechanical Engineering from the University of Craiova, Romania in 1988, the PhD from the University of Petrosani, Romania in 2002, followed by a research fellowship in Urology at the Johns Hopkins University. Between 1991–1994 he was Assistant Professor at the University of Craiova and Lecturer since 1994. In 2002 he joined the Urology Robotics research group at Johns Hopkins and currently is Research Associate Professor. Dr. Petrisor's specialty is design and manufacturing of medical devices. His bibliography includes numerous articles, presentations, and 4 patents of invention.



Changhan Jun received a B.S. degree from the Department of Mechanical, Materials and Aerospace Engineering, Illinois Institute of Technology, Chicago, IL, USA in 2010. He received a M.S. degree at the Department of Mechanical Engineering, Johns Hopkins University, Baltimore, MD, USA in 2013. Since 2012, he studies toward a Ph.D. degree at Urology Robotics Laboratory, Johns Hopkins University, Baltimore, MD, USA. His research interests include image-guided robots and medical devices.



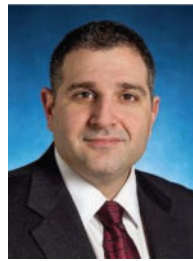
Sunghwan Lim received the B.S. degree from the Department of Mechanical Engineering and Materials Science, Yokohama National University, and the M.S degree from the Department of Bioengineering, The University of Tokyo, Japan, in 2008 and 2010, respectively. From 2010 to 2012, he was an Instructor at the Gondar Polytechnic College, Ethiopia. From 2012 to 2014 he was Research Scientist at the Biomedical Research Institute, Korea Institute of Science and Technology, Seoul, Korea. He is currently working toward the Ph.D. degree at The Johns Hopkins University, Baltimore, MD, USA. His research interests include image-guided medical robots and medical imaging.



Mark Ball completed his undergraduate studies in biochemistry and molecular biology at Centre College and his medical training, internship and urology residency at Johns Hopkins. He is currently a fellow in urologic oncology at the National Cancer Institute at the National Institutes of Health. His academic focus is understanding the tumor biology of urologic malignancies.



Ashley Ross completed his MD and PhD degrees as well as urological training at the Johns Hopkins School of Medicine where he currently serves as an Assistant Professor in the Departments of Urology, Oncology and Pathology. Dr. Ross's clinical and research efforts focus on prostate cancer and he leads institutional efforts in prostate cancer as the Director of the Brady Urology Prostate Cancer Program. He is also an active member of the Sidney Kimmel Comprehensive Cancer Center at Johns Hopkins where he is co-director of the prostate cancer multi-disciplinary clinic and director of the high risk prostate cancer clinic. He is an active surgeon scientist and leads several clinical trials exploring novel therapeutic and diagnostic approaches for prostate cancer. Dr. Ross's research efforts have been recognized and supported by the Johns Hopkins Clinical Scientist Award, Department of Defense Prostate Cancer PTR A Award, Patrick C. Walsh Prostate Cancer Research Award, and Prostate Cancer Foundation Young Investigator Award.



Katarzyna J. Macura, MD, PhD, FACR, FSCBTMR is a Professor in the Johns Hopkins Medicine departments of Radiology and Radiological Science, Oncology and Urology. She is Assistant Director for the Imaging Translational Program of the Johns Hopkins Institute for Clinical and Translational Research (ICTR). Dr. Macura earned her medical degree from the Medical University of Lodz in Poland. She completed a residency in diagnostic radiology at the Medical College of Georgia and a fellowship in cross-sectional body imaging at the Johns Hopkins University. Dr. Macura is a Fellow of the American College of Radiology and the Society of Computed Body Tomography and Magnetic Resonance. Dr. Macura established a clinical and research prostate imaging program at Hopkins focusing on magnetic resonance imaging.



References

1. Kelloff GJ, Choyke P, Coffey DS. Challenges in clinical prostate cancer: role of imaging. *AJR Am J Roentgenol.* 2009; 192:1455–70. [PubMed: 19457806]
2. Resnick MJ, Lee DJ, Magerfleisch L, Vanarsdalen KN, Tomaszewski JE, Wein AJ, Malkowicz SB, Guzzo TJ. Repeat prostate biopsy and the incremental risk of clinically insignificant prostate cancer. *Urology.* 2011; 77:548–52. <http://www.ncbi.nlm.nih.gov/pubmed/21215436>. [PubMed: 21215436]
3. Han M, Chang D, Kim C, Lee BJ, Zuo Y, Kim HJ, Petrisor D, Trock B, Partin AW, Rodriguez R, Carter HB, Allaf M, Kim J, Stoianovici D. Geometric Evaluation of Systematic Transrectal Ultrasound Guided Prostate Biopsy. *Journal of Urology.* 2012; 188:2404–9. <http://urobotics.urology.jhu.edu/pub/2012-han-jurol.pdf>. [PubMed: 23088974]
4. Hricak H, Choyke PL, Eberhardt SC, Leibel SA, Scardino PT. Imaging prostate cancer: a multidisciplinary perspective. *Radiology.* 2007; 243:28–53. [PubMed: 17392247]
5. Villers A, Marliere F, Ouzzane A, Puech P, Lemaitre L. MRI in addition to or as a substitute for prostate biopsy: the clinician's point of view. *Diagn Interv Imaging.* 2012; 93:262–7. <http://www.ncbi.nlm.nih.gov/pubmed/22465789>. [PubMed: 22465789]
6. Mozer P, Partin AW, Stoianovici D. Robotic Image-Guided Needle Interventions of the Prostate. *Reviews in Urology.* 2009; 11:7–15. <http://urobotics.urology.jhu.edu/pub/2009-mozer-revuro.pdf>. [PubMed: 19390670]
7. Xu S, Kruecker J, Turkbey B, Glossop N, Singh AK, Choyke P, Pinto P, Wood BJ. Real-time MRI-TRUS fusion for guidance of targeted prostate biopsies. *Comput Aided Surg.* 2008; 13:255–64. <http://www.ncbi.nlm.nih.gov/pubmed/18821344>. [PubMed: 18821344]
8. Frye TP, Pinto PA, George AK. Optimizing Patient Population for MP-MRI and Fusion Biopsy for Prostate Cancer Detection. *Curr Urol Rep.* 2015; 16:50. <http://www.ncbi.nlm.nih.gov/pubmed/26063625>. [PubMed: 26063625]
9. Thoma C. Prostate cancer: MRI/TRUS fusion outperforms standard and combined biopsy approaches. *Nat Rev Urol.* 2015; 12:119. <http://www.ncbi.nlm.nih.gov/pubmed/25687268>. [PubMed: 25687268]
10. Stoianovici D. Technology Advances for Prostate Biopsy and Needle Therapies. Editorial. *Journal of Urology.* 2012; 188:1074–5. <http://urobotics.urology.jhu.edu/pub/2012-stoianovici-jurol.pdf>. [PubMed: 22901579]
11. Taylor RH, Stoianovici D. Medical robotics in computer-integrated surgery. *IEEE Transactions on Robotics and Automation.* 2003; 19:765–781. <http://urobotics.urology.jhu.edu/pub/2003-taylor-ieeeextra.pdf>.
12. Blumberg KD, Catalano JB, Cotler JM, Balderston RA. The pullout strength of titanium alloy MRI-compatible and stainless steel MRI-incompatible Gardner-Wells tongs. *Spine (Phila Pa 1976).* 1993; 18:1895–6. <http://www.ncbi.nlm.nih.gov/pubmed/8235879>. [PubMed: 8235879]
13. Gassert R, Burdet E, Chinzei K. MRI-Compatible Robotics. *IEEE Eng Med Biol Mag.* 2008; 27:12–4. <http://www.ncbi.nlm.nih.gov/pubmed/18519176>.
14. Stoianovici D, Kim C, Srimathveeravalli G, Sebrecht P, Petrisor D, Coleman J, Solomon SB, Hricak H. MRI-Safe Robot for Endorectal Prostate Biopsy. *Ieee-Asme Transactions on Mechatronics.* 2014; 19:1289–1299. <http://urobotics.urology.jhu.edu/pub/2014-stoianovici-tmech.pdf>.

15. Su H, Camilo A, Cole GA, Hata N, Tempany CM, Fischer GS. High-field MRI-compatible needle placement robot for prostate interventions. *Stud Health Technol Inform*. 2011; 163:623–9. [PubMed: 21335868]
16. Fischer GS, Cole G, Su H. Approaches to creating and controlling motion in MRI. *Conf Proc IEEE Eng Med Biol Soc*. 2011; 2011:6687–90. <http://www.ncbi.nlm.nih.gov/pubmed/22255873>. [PubMed: 22255873]
17. Stoianovici D. Multi-Imager Compatible Actuation Principles in Surgical Robotics. *International Journal of Medical Robotics and Computer Assisted Surgery*. 2005; 1:86–100. <http://urology.jhu.edu/urobotics/pub/2005-stoianovici-MRCASJ.pdf>. [PubMed: 17518382]
18. Beyersdorff D, Winkel A, Hamm B, Lenk S, Loening SA, Taupitz M. MR imaging-guided prostate biopsy with a closed MR unit at 1.5 T: initial results. *Radiology*. 2005; 234:576–81. [PubMed: 15616117]
19. Susil RC, Menard C, Krieger A, Coleman JA, Camphausen K, Choyke P, Fichtinger G, Whitcomb LL, Coleman CN, Atalar E. Transrectal prostate biopsy and fiducial marker placement in a standard 1.5T magnetic resonance imaging scanner. *J Urol*. 2006; 175:113–20. <http://www.ncbi.nlm.nih.gov/pubmed/16406885>. [PubMed: 16406885]
20. Cepek J, Chronik BA, Lindner U, Trachtenberg J, Davidson SR, Bax J, Fenster A. A system for MRI-guided transperineal delivery of needles to the prostate for focal therapy. *Med Phys*. 2013; 40:012304. <http://www.ncbi.nlm.nih.gov/pubmed/23298109>. [PubMed: 23298109]
21. Wang Y, Cole GA, Su H, Pilitsis JG, Fischer GS. MRI compatibility evaluation of a piezoelectric actuator system for a neural interventional robot. *Conf Proc IEEE Eng Med Biol Soc*. 2009; 2009:6072–5. [PubMed: 19964890]
22. Krieger A, Song SE, Cho NB, Iordachita I, Guion P, Fichtinger G, Whitcomb LL. Development and Evaluation of an Actuated MRI-Compatible Robotic System for MRI-Guided Prostate Intervention. *IEEE ASME Trans Mechatron*. 2012; 18:273–284. [PubMed: 23326181]
23. Song SE, Hata N, Iordachita I, Fichtinger G, Tempany C, Tokuda J. A workspace-orientated needle-guiding robot for 3T MRI-guided transperineal prostate intervention: evaluation of in-bore workspace and MRI compatibility. *Int J Med Robot*. 2013; 9:67–74. <http://www.ncbi.nlm.nih.gov/pubmed/22492680>. [PubMed: 22492680]
24. Tokuda J, Tuncali K, Iordachita I, Song SE, Fedorov A, Oguro S, Lasso A, Fennessy FM, Tempany CM, Hata N. In-bore setup and software for 3T MRI-guided transperineal prostate biopsy. *Phys Med Biol*. 2012; 57:5823–40. <http://www.ncbi.nlm.nih.gov/pubmed/22951350>. [PubMed: 22951350]
25. Sutherland GR, Latour I, Greer AD. Integrating an image-guided robot with intraoperative MRI: a review of the design and construction of neuroArm. *IEEE Eng Med Biol Mag*. 2008; 27:59–65. <http://www.ncbi.nlm.nih.gov/pubmed/18519183>. [PubMed: 18519183]
26. Song SE, Tokuda J, Tuncali K, Tempany CM, Zhang E, Hata N. Development and preliminary evaluation of a motorized needle guide template for MRI-guided targeted prostate biopsy. *IEEE Trans Biomed Eng*. 2013; 60:3019–27. <http://www.ncbi.nlm.nih.gov/pubmed/23335658>. [PubMed: 23335658]
27. Zangos S, Herzog C, Eichler K, Hammerstingl R, Lukoschek A, Guthmann S, Gutmann B, Schoepf UJ, Costello P, Vogl TJ. MR-compatible assistance system for puncture in a high-field system: device and feasibility of transgluteal biopsies of the prostate gland. *Eur Radiol*. 2007; 17:1118–24. http://www.ncbi.nlm.nih.gov/entrez/query.fcgi?cmd=Retrieve&db=PubMed&dopt=Citation&list_uids=17031454. [PubMed: 17031454]
28. Schouten MG, Ansems J, Renema WK, Bosboom D, Scheenen TW, Futterer JJ. The accuracy and safety aspects of a novel robotic needle guide manipulator to perform transrectal prostate biopsies. *Med Phys*. 2010; 37:4744–50.
29. Stoianovici D, Patriciu A, Mazilu D, Petrisor D, Kavoussi L. A New Type of Motor: Pneumatic Step Motor. *IEEE/ASME Transactions on Mechatronics*. 2007; 12:98–106. 2008 Best Paper Award of the Journal. <http://urobotics.urology.jhu.edu/pub/2007-stoianovici-tmech.pdf>. [PubMed: 21528106]
30. Stoianovici D, Song D, Petrisor D, Ursu D, Mazilu D, Muntener M, Schar M, Patriciu A. “MRI Stealth” Robot for Prostate Interventions. *Minimally Invasive Therapy & Allied Technologies*.

- 2007; 16:241–248. <http://urobotics.urology.jhu.edu/pub/2007-stoianovici-mitat.pdf>. [PubMed: 17763098]
31. Muntener M, Patriciu A, Petrisor D, Mazilu D, Kavoussi L, Cleary K, Stoianovici D. Magnetic Resonance Imaging Compatible Robotic System for Fully Automated Brachytherapy Seed Placement. *Urology*. 2006; 68:1313–1317. <http://urobotics.urology.jhu.edu/pub/2006-muntener-urology.pdf>. [PubMed: 17169653]
 32. Muntener M, Patriciu A, Petrisor D, Schar M, Ursu D, Song D, Stoianovici D. Transperineal prostate intervention: robot for fully automated MR imaging–system description and proof of principle in a canine model. *Radiology*. 2008; 247:543–549. <http://urobotics.urology.jhu.edu/pub/2008-muntener-radiology.pdf>. [PubMed: 18430882]
 33. Althoefer K. MRI-safe robots. Why are they not yet routinely used? *BJU Int*. 2014; 113:975–6. <http://www.ncbi.nlm.nih.gov/pubmed/24612038>. [PubMed: 24612038]
 34. van den Bosch MR, Moman MR, van Vulpen M, Battermann JJ, Duiveman E, van Schelven LJ, de Leeuw H, Lagendijk JJ, Moerland MA. MRI-guided robotic system for transperineal prostate interventions: proof of principle. *Phys Med Biol*. 2010; 55:N133–40. <http://www.ncbi.nlm.nih.gov/pubmed/20145293>. [PubMed: 20145293]
 35. Yakar D, Schouten MG, Bosboom DG, Barentsz JO, Scheenen TW, Futterer JJ. Feasibility of a pneumatically actuated MR-compatible robot for transrectal prostate biopsy guidance. *Radiology*. 2011; 260:241–7. [PubMed: 21406625]
 36. Zangos S, Melzer A, Eichler K, Sadighi C, Thalhammer A, Bodelle B, Wolf R, Gruber-Rouh T, Proschek D, Hammerstingl R, Muller C, Mack MG, Vogl TJ. MR-compatible assistance system for biopsy in a high-field-strength system: initial results in patients with suspicious prostate lesions. *Radiology*. 2011; 259:903–10. <http://www.ncbi.nlm.nih.gov/pubmed/21364080>. [PubMed: 21364080]
 37. Song SE, Tuncali K, Tokuda J, Fedorov A, Penzkofer T, Fennessy F, Tempany C, Yoshimitsu K, Magill J, Hata N. Workflow Assessment of 3T MRI-guided Transperineal Targeted Prostate Biopsy using a Robotic Needle Guidance. *Medical Imaging 2014: Image-Guided Procedures, Robotic Interventions, and Modeling*. 2014; 9036 <Go to ISI>://000348029400038.
 38. Tilak G, Tuncali K, Song SE, Tokuda J, Olubiyi O, Fennessy F, Fedorov A, Penzkofer T, Tempany C, Hata N. 3T MR-guided in-bore transperineal prostate biopsy: A comparison of robotic and manual needle-guidance templates. *J Magn Reson Imaging*. 2015; 42:63–71. <http://www.ncbi.nlm.nih.gov/pubmed/25263213>. [PubMed: 25263213]
 39. Patriciu A, Petrisor D, Muntener M, Mazilu D, Schar M, Stoianovici D. Automatic Brachytherapy Seed Placement under MRI Guidance. *IEEE Transactions on Biomedical Engineering*. 2007; 54:1499–1506. <http://urobotics.urology.jhu.edu/pub/2007-patriciu-tbme.pdf>. [PubMed: 17694871]
 40. Ball MW, Ross AE, Ghabili K, Kim C, Jun C, Petrisor D, Epstein JI, Macura K, Stoianovici D, Allaf ME. Safety and Feasibility of Robot-Assisted Direct MRI-Guided Transperineal Prostate Biopsy. *Urology*. 2016 under review.
 41. M. R. S. Expert Panel on. Kanal E, Barkovich AJ, Bell C, Borgstede JP, Bradley WG Jr, Froelich JW, Gimbel JR, Gosbee JW, Kuhni-Kaminski E, Larson PA, Lester JW Jr, Nyenhuis J, Schaefer DJ, Sebek EA, Weinreb J, Wilkoff BL, Woods TO, Lucey L, Hernandez D. ACR guidance document on MR safe practices: 2013. *J Magn Reson Imaging*. 2013; 37:501–30. <http://www.ncbi.nlm.nih.gov/pubmed/23345200>. [PubMed: 23345200]
 42. Kanal E, Barkovich AJ, Bell C, Borgstede JP, Bradley WG Jr, Froelich JW, Gilk T, Gimbel JR, Gosbee J, Kuhni-Kaminski E, Lester JW Jr, Nyenhuis J, Parag Y, Schaefer DJ, Sebek-Scoumis EA, Weinreb J, Zaremba LA, Wilcox P, Lucey L, Sass N. ACR guidance document for safe MR practices: 2007. *AJR Am J Roentgenol*. 2007; 188:1447–74. [PubMed: 17515363]
 43. CFR - Code of Federal Regulations Title 21, Part 812 Investigational Device Exemptions. Apr 1. 2015 <http://www.accessdata.fda.gov/SCRIPTS/cdrh/cfdocs/cfCFR/CFRSearch.cfm?CFRPart=812>
 44. U.S. Food and Drug Administration. IDE Application. <http://www.fda.gov/MedicalDevices/DeviceRegulationandGuidance/HowtoMarketYourDevice/InvestigationalDeviceExemptionIDE/ucm046706.htm>
 45. Fichtinger G, De Weese TL, Patriciu A, Tanacs A, Mazilu D, Anderson JH, Masamune K, Taylor RH, Stoianovici D. System for robotically assisted prostate biopsy and therapy with intraoperative

- CT guidance. *Academic Radiology*. 2002; 9:60–74. <http://urobotics.urology.jhu.edu/pub/2002-fichtinger-acrad.pdf>. [PubMed: 11918360]
46. Cleary, K., Zigmundb, B., Banovaca, F., Whitec, C., Stoianovici, D. Robotically assisted lung biopsy under CT fluoroscopy: lung cancer screening and phantom study. presented at Computer Assisted Radiology and Surgery (CARS 2005). 2005. <http://urobotics.urology.jhu.edu/pub/2005-cleary-CARS.pdf>
47. Webster RJ, Kim JS, Cowan NJ, Chirikjian GS, Okamura AM. Nonholonomic modeling of needle steering. *International Journal of Robotics Research*. 2006; 25:509–525. <Go to ISI>://WOS: 000238146600006.
48. Chen Y, Kwok KW, Tse ZT. An MR-conditional high-torque pneumatic stepper motor for MRI-guided and robot-assisted intervention. *Ann Biomed Eng*. 2014; 42:1823–33. <http://www.ncbi.nlm.nih.gov/pubmed/24957635>. [PubMed: 24957635]
49. Tokuda J, Song SE, Fischer GS, Iordachita II, Seifabadi R, Cho NB, Tuncali K, Fichtinger G, Tempany CM, Hata N. Preclinical evaluation of an MRI-compatible pneumatic robot for angulated needle placement in transperineal prostate interventions. *Int J Comput Assist Radiol Surg*. 2012; 7:949–57. <http://www.ncbi.nlm.nih.gov/pubmed/22678723>. [PubMed: 22678723]
50. Blumenfeld P, Hata N, Di Maio S, Zou K, Haker S, Fichtinger G, Tempany CM. Transperineal prostate biopsy under magnetic resonance image guidance: a needle placement accuracy study. *J Magn Reson Imaging*. 2007; 26:688–94. <http://www.ncbi.nlm.nih.gov/pubmed/17729363>. [PubMed: 17729363]
51. Ukimura O, Desai MM, Palmer S, Valencerina S, Gross M, Abreu AL, Aron M, Gill IS. 3-Dimensional elastic registration system of prostate biopsy location by real-time 3-dimensional transrectal ultrasound guidance with magnetic resonance/transrectal ultrasound image fusion. *J Urol*. 2012; 187:1080–6. <http://www.ncbi.nlm.nih.gov/pubmed/22266005>. [PubMed: 22266005]
52. Jun, C., Kim, C., Chang, D., Decker, R., Petrisor, D., Stoianovici, D. Beveled Needle Trajectory Correction. Engineering and Urology Society, 28th Annual Meeting; San Diego, CA. 2013; http://engineering-urology.org/am/28EUS_2013.pdf
53. Badaan S, Petrisor D, Kim C, Mozer P, Mazilu D, Gruionu L, Patriciu A, Cleary K, Stoianovici D. Does needle rotation improve lesion targeting? *International Journal of Medical Robotics and Computer Assisted Surgery*. 2011; 7:138–147. <http://urobotics.urology.jhu.edu/pub/2011-badaan-ijmrcas.pdf>. [PubMed: 21360796]

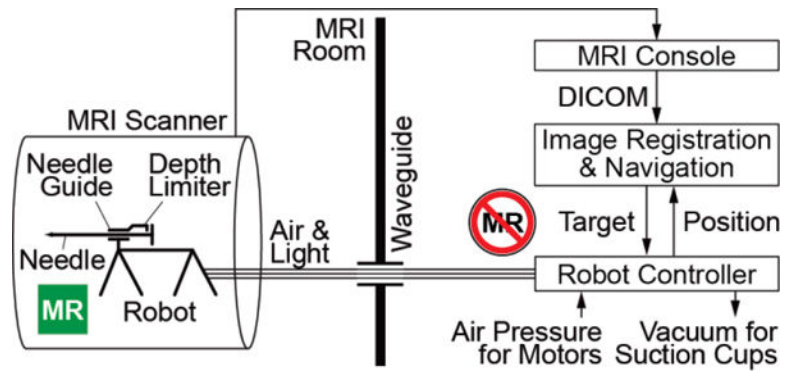


Figure 1.
System schematic

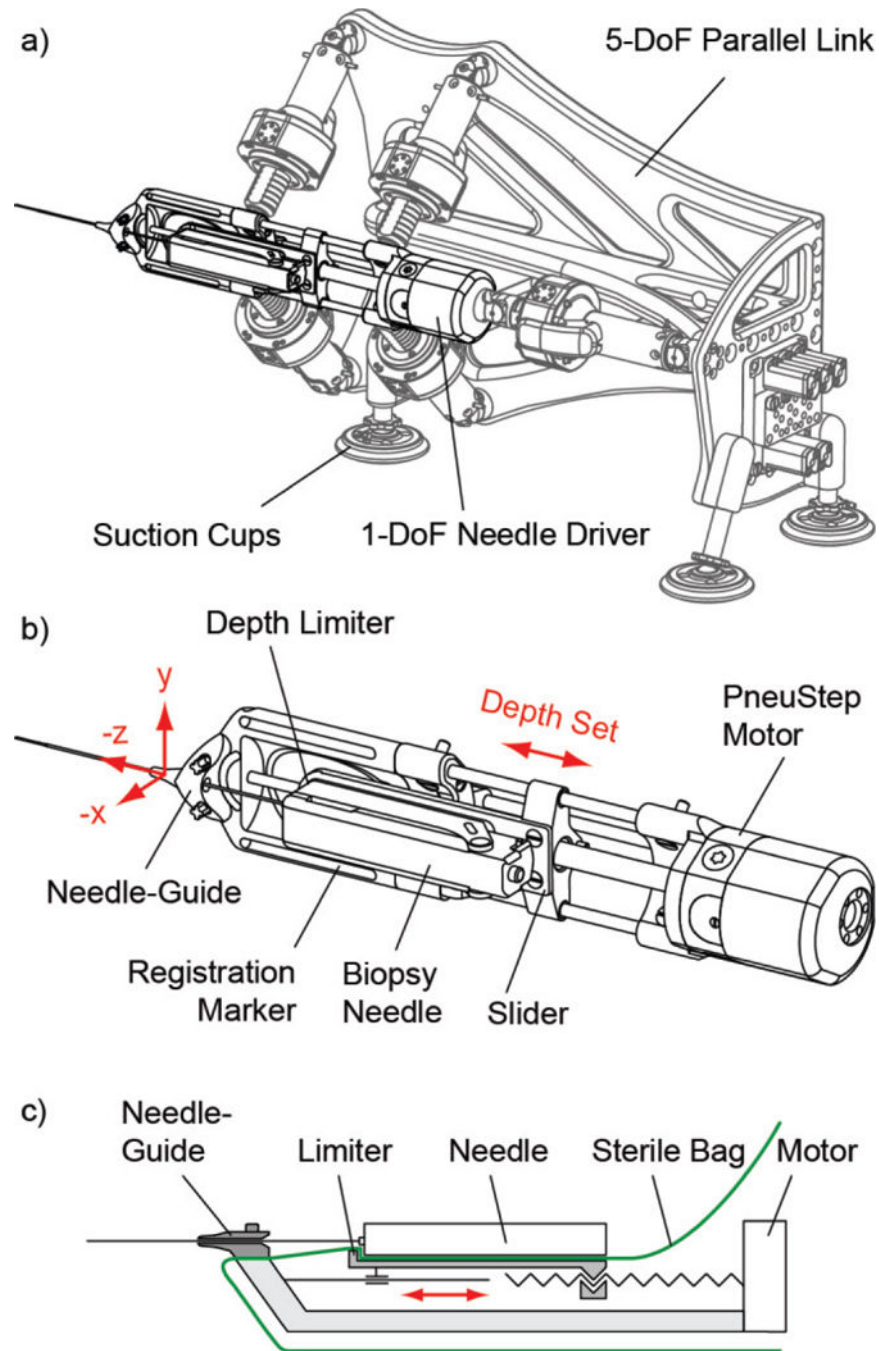


Figure 2.
 a) The robot, b) Needle-driver, and c) Schematic of the needle-driver

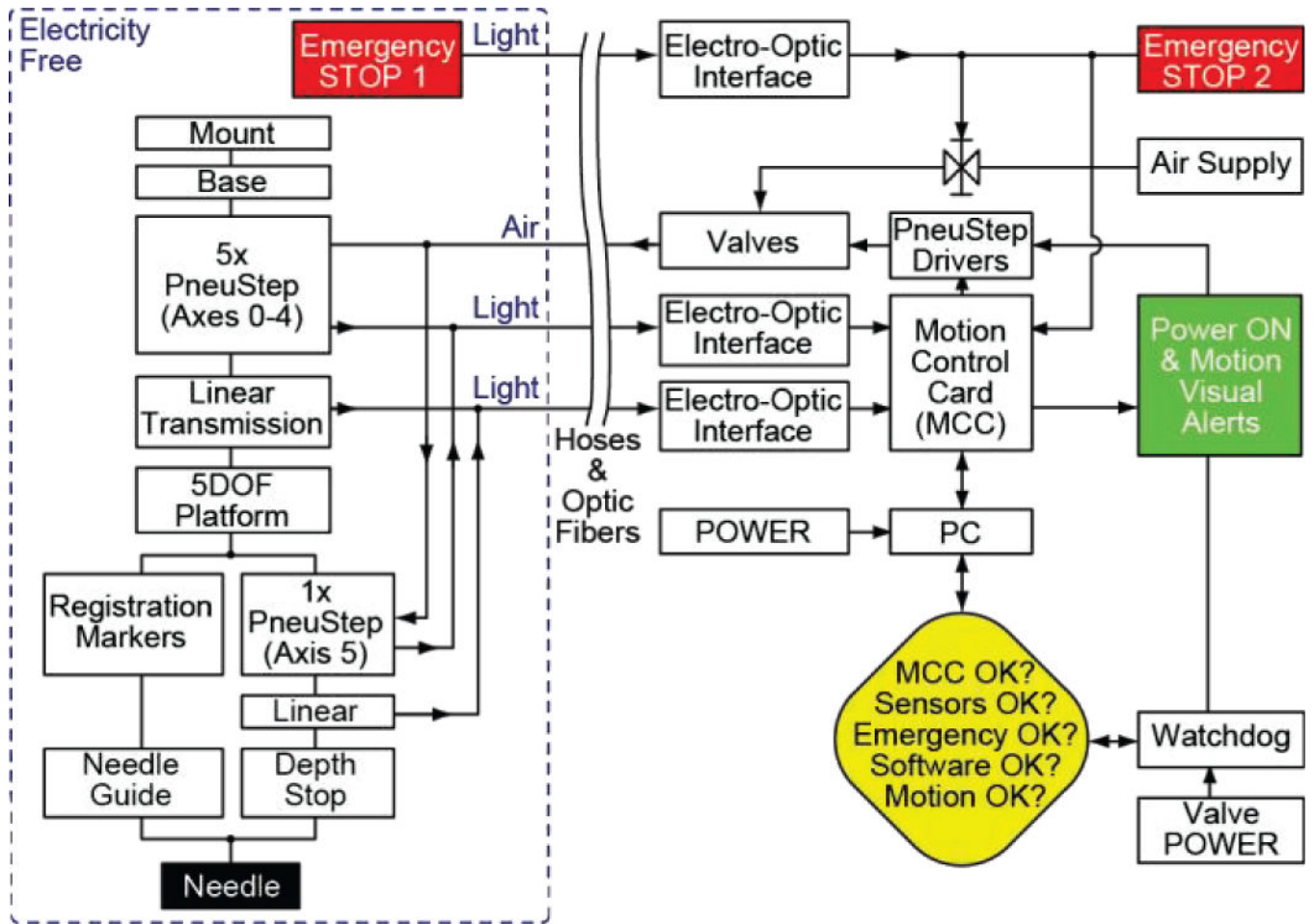


Figure 3. Block diagram of the robot controller

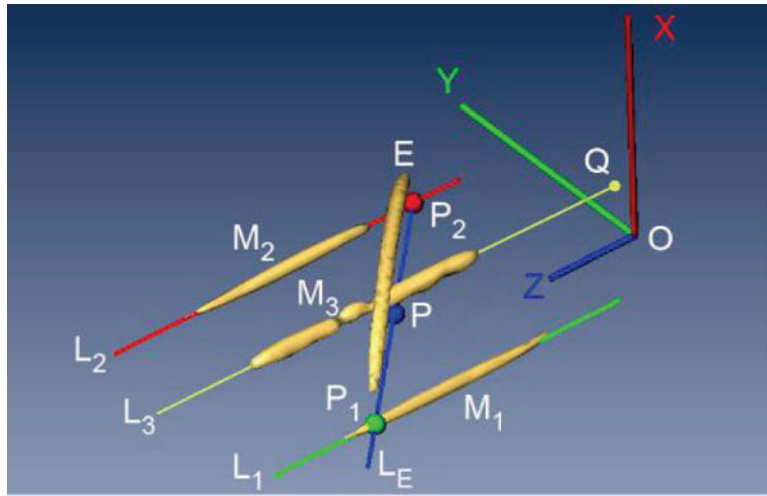


Figure 4.
Registration markers and image-to-model

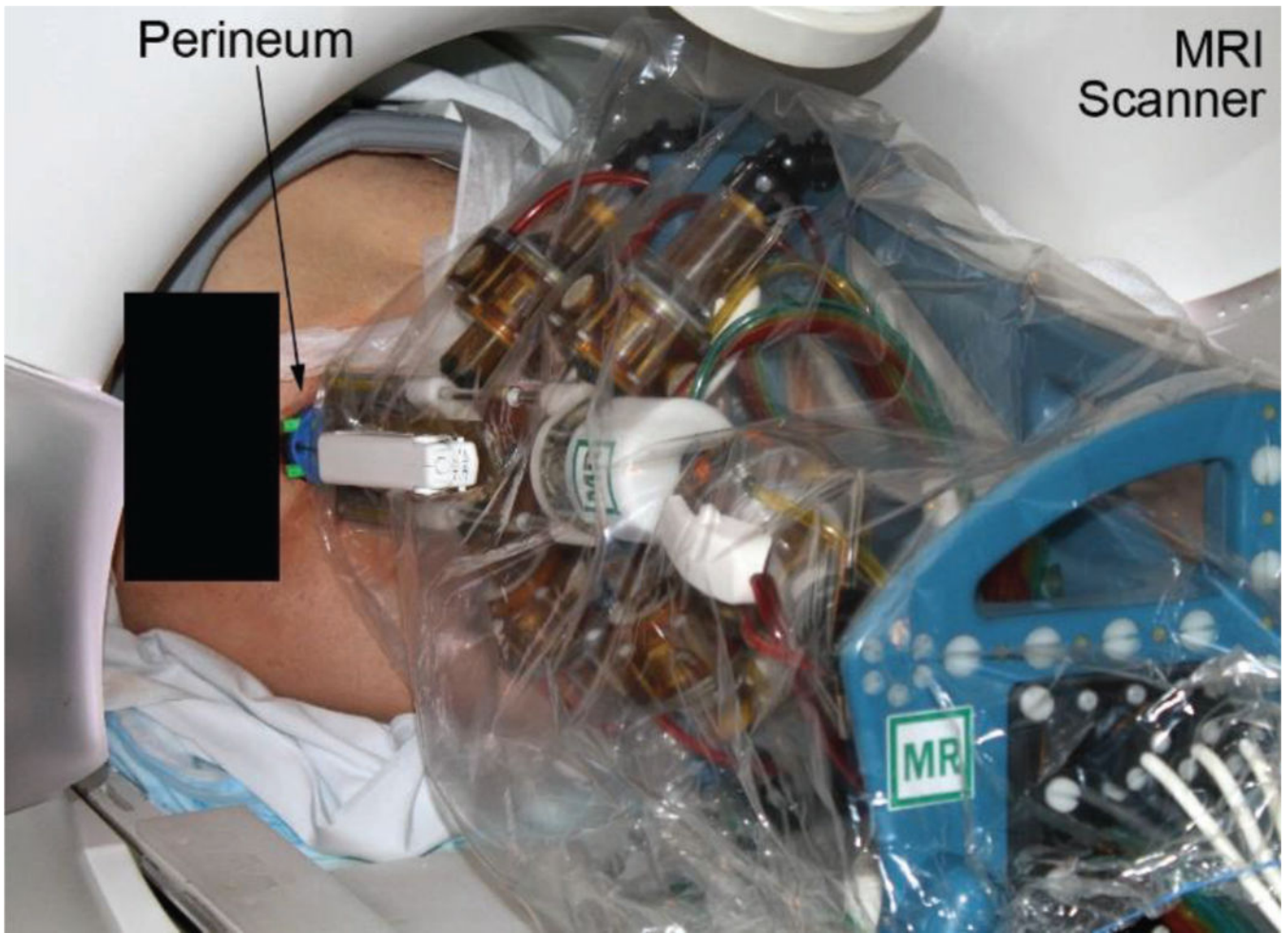





Figure 5.
Patient and robot in the MRI scanner

Table 1

ASTM F2503-13 classification and marking for the MR environment

<p>MR Safe</p> 	<p>An item that poses no known hazards resulting from exposure to any MR environment. MR Safe items are composed of materials that are electrically nonconductive, nonmetallic, and nonmagnetic. An item composed entirely of electrically nonconductive, nonmetallic and nonmagnetic materials may be determined to be MR Safe by providing a scientifically based rationale rather than test data.</p>
<p>MR Conditional</p> 	<p>An item with demonstrated safety in the MR environment within defined conditions. At a minimum, address the conditions of the static magnetic field, the switched gradient magnetic field and the radiofrequency fields. Additional conditions, including specific configurations of the item, may be required. Supplementary Marking — additional information that, in association with a marking as “MR Conditional,” states via additional language the conditions in which an item can be used safely within the MR environment.</p>
<p>MR Unsafe</p> 	<p>An item which poses unacceptable risks to the patient, medical staff or other persons within the MR environment.</p>

Author Manuscript

Author Manuscript

Author Manuscript

Author Manuscript

Table 2

Image-to-model registration precision and accuracy

Image Set	Angular [°]	Offset [mm]
Precision	0.12	0.25
Accuracy	0.91	0.31

Author Manuscript

Author Manuscript

Author Manuscript

Author Manuscript

Table 3

MRI based needle targeting precision and accuracy over 30 biopsy sites

	3D	Normal to the needle
Accuracy [mm]	2.97	2.55
Precision [mm]	1.50	1.59
Trajectory corrections	0	

Author Manuscript

Author Manuscript

Author Manuscript

Author Manuscript

Table 4

Device related outcome variables

	Average (SD)
Unsuccessful attempts to target a site	0
Device setup time [min]	8.4 (3.4)
Image registration [min]	8.4 (5.8)
Align needle-guide on target/site [min]	1.6 (1.4)
Total biopsy time/site [min]	9.7 (1.0)
Operation of the device [1–5, 1 excellent]	1.5 (0.3)
Image Deterioration [1–5, 1 unperceivable]	1.0 (0.0)

Author Manuscript

Author Manuscript

Author Manuscript

Author Manuscript